Composite Structures 139 (2016) 243–253

Contents lists available at ScienceDirect

Composite Structures

journal homepage: www.elsevier.com/locate/compstruct

Buckling behavior of variable-stiffness composite laminates manufactured by the tow-drop method

A. Marouene [a,*], R. Boukhili [a], J. Chen [b], A. Yousefpour [b]

[a] Polytechnique Montreal, Department of Mechanical Engineering, 2900 Boulevard Edouard-Montpetit, Montreal, Quebec H3C 3A7, Canada
[b] Aerospace Manufacturing Technology Center, Institute for Aerospace Research, National Research Council Canada, 5145 Decelles Avenue, Montreal, Quebec H3T 2B2, Canada

ARTICLE INFO

Article history:
Available online 30 December 2015

Keywords:
Automated fiber placement
Buckling
Gaps/overlaps
Tow-drop
Variable-stiffness panels

ABSTRACT

The current investigation deals with the buckling behavior of variable-stiffness composite panels manufactured by the automated fiber placement (AFP) process. In order to minimize the occurrence of AFP-inherent defects as gaps and overlaps, the so-called tow-drop method was adopted. Compression-buckling tests were performed on large panels containing gaps or overlaps under simply-supported boundary conditions. The specific responses of the out-of-plane deflections, which were tracked by four laser sensors focused on the axial centerline of the panels during compression loading, were explained by the measured initial geometric curvatures, which were characteristic of variable-stiffness panels. The tracking of the in-plane strains using sixteen strain gauges located strategically on the panels confirmed that the presence of gaps and overlaps does not affect the symmetry of variable-stiffness panels. Finally, it was established that the tow-drop method significantly improved the structural performance in terms of the pre-buckling stiffness, buckling load, and the failure load while keeping minimal geometric disturbances.

© 2015 The Authors. Published by Elsevier Ltd. This is an open access article under the CC BY-NC-ND license (http://creativecommons.org/licenses/by-nc-nd/4.0/).

1. Introduction

Automated fiber placement (AFP) is a leading technology for manufacturing large and complex aerospace composite structures and is presently the preferred process for producing modern aircraft, such as the Boeing 787, the Airbus 350 XWB, and the Bombardier C-Series. A recent review paper [1] discussed the development of the automated prepreg processes used for manufacturing composites, including the AFP process. Although the AFP process is primarily used for manufacturing composite structures with straight fibers (i.e., constant-stiffness laminates), it offers the possibility of steering individual fiber tows along curvilinear paths. This manufacturing feature has widely opened the way to what are known as variable-stiffness laminates [2]. Variable-stiffness laminates allow designers to reinforce and enhance the structural properties against the load direction, which is significantly desirable to produce aircraft structures. Several research studies on the design and optimization of composite materials have demonstrated the potential of the variable-stiffness design to improve the in-plane stiffness (e.g. [3–5]), buckling resistance (e.g. [6–8]), strength (e.g. [9–11]), vibration response (e.g. [12–14]) and bending properties (e.g. [15–17]). However, the manufacturing of the variable-stiffness laminates reveals misgivings associated with specific inherent defects induced by the fiber steering, referred to as gaps and overlaps; the effects of these defects on the structural performance of composite laminates are not yet well understood. Therefore, elucidating the effects of these defects is essential for the development of this promising design.

In the open-literature, there are numerous experimental and numerical studies which address the effects of gaps and/or overlaps on the mechanical properties of constant-stiffness laminates. Among them, Sawicki and Minguet [18] investigated the decrease in the compressive strength of straight-fiber laminates with intra-ply overlap and gap defects. Turoski [19] performed numerical and experimental analyses to investigate the effects of the number of gaps on the ultimate strength of 32-ply carbon/epoxy composite plates under uniaxial tensile and compressive loads. Croft et al. [20] addressed an experimental approach to understand the effects of four different defect configurations, namely, gaps, overlaps, twisted tows, and half gaps/overlaps, on the mechanical performance of laminate composites. Legay et al. [21] examined the effects of gaps and overlaps on the low-velocity impact response of AFP-manufactured 24-ply quasi-isotropic carbon/epoxy laminates. They examined the damage-initiation load, the peak impact load, the absorbed energy, the damage area, and the compression-

* Corresponding author.

http://dx.doi.org/10.1016/j.compstruct.2015.12.025
0263-8223/© 2015 The Authors. Published by Elsevier Ltd.
This is an open access article under the CC BY-NC-ND license (http://creativecommons.org/licenses/by-nc-nd/4.0/).

after-impact strength. Fayazbakhsh et al. [22] performed a finite element analysis to investigate the effects of gaps and overlaps on the compressive strength of a quasi-isotropic laminate with a $[45/0/-45/90]_{3s}$ lay-up. They used the experimental data available in the literature to validate the FE model and results. A reasonable agreement between the experimental and numerical results was reported.

Although it is fairly easy to find experimental data on the effects of the AFP process-induced defects on the mechanical characteristics of constant-stiffness composites, most published studies on variable-stiffness composite laminates have involved numerical simulations (e.g. [10,23,24]), and there is a lack of experimental data related to these inherent defects (i.e., gaps and overlaps), as reported in Ref. [25]. Wu et al. [26,27] performed numerical and experimental analyses on the buckling behavior of two-steered composite panels (i.e., with and without overlaps) subjected to uniaxial compression. Jegley et al. [28,29] performed compression and shear tests on tow-steered panels with a central circular cutout. The results of these studies indicated that the overall elastic properties of variable-stiffness panels with gaps and overlaps were significantly better than those of their constant-stiffness counterparts. However, it should be pointed out that, in the previous studies[26–29], the strategy adopted for manufacturing the tested panels, referred to as the tow-overlapping method [30], led to a significant amount of overlaps within the panels. The manufactured panels were quite unsymmetrical, since they had one smooth side (the one that was against the mold surface) and one bumpy side, owing to the excessive amount of overlaps and thickness build-up. Such geometry is generally undesirable for aerodynamic control surfaces in aeronautical applications, like in aircraft wings, which control the air flow rate and aircraft lift. Previous authors [26–29] have used the staggering technique, which involves offsetting the origin of the main path for each ply by a small distance, during the manufacturing process, in order to prevent the clustering of the AFP defects. Nevertheless, after consolidation, the cured variables-stiffness panels presented large initial geometrical imperfections compared to the constant-stiffness panel used as the baseline panel. To counter this, Wu et al. [26] forced the supported panels' edges straight during the compression test. This interference during testing probably affects the buckling behavior of the panels, as the performance of variable-stiffness panels is highly dependent on the boundary conditions [5].

In contrast with the tow-overlapping method, another manufacturing method can be used to reduce the geometrical anomalies and minimize the amount of defects induced in the AFP-manufactured variable-stiffness panels. This method, which involves cutting the fiber-tows to avoid the formation of an excessive amount of AFP defects, referred to as tow-drop method. In practice, several design strategies can be adopted when the tow-drop method is employed. These strategies can be classified on the basis of the «coverage percentage» parameter [31]. In the strategy corresponding to 0% coverage (i.e., complete gap), the tow is dropped as soon as one edge of the tow reaches the limiting curve (e.g. an adjacent course or the bounding edge of the laminate); this results in small triangular resin-rich areas (i.e., gaps). In opposite, in the strategy corresponding to 100% coverage (i.e., complete overlap), the tow is dropped when both edges of the tow cross the limiting curve; this results in small areas of triangular overlap. Furthermore, intermediate scenarios are also possible, in which the coverage percentage lies between 0% and 100% (see [31] for details).

The current investigation aimed to quantify the effects of the AFP process-induced defects on the buckling and post-buckling characteristics of rectangular, simply-supported, variable-stiffness panels subjected to uniform in-plane displacement. For this purpose, two optimal variable-stiffness panels with the lowest possible amount of AFP defects were manufactured using the tow-drop method: one corresponded to 0% coverage (i.e., with complete gaps) and the other corresponded to 100% coverage (i.e., with complete overlaps). A special fixture was designed and manufactured to ensure the simply-supported boundary conditions at all of the panels' edges during experiment. The buckling characteristics of the variable-stiffness panels were determined, and the results were compared with those obtained for a constant-stiffness panel (i.e., defect-free quasi-isotropic baseline panel). This experimental work is part of the COMP-413 project [5,20,23,24], intended to optimize the design of steered-tow composite structures by taking into account the AFP process-induced defects. Ref. [5] examined the multi-objective optimization of the in-plane stiffness and buckling load of a flat composite plate with variable stiffness using the surrogated NSGA-II approach (NSGA-II: Non-dominated Sorting Genetic Algorithm-II). The flow chart of the surrogate-based optimization defined in Ref. [5] served to propose two optimized variable-stiffness composite panels intended to be manufactured using a Viper 4000 AFP machine.

2. Experimental procedures

2.1. Material and test panel manufacturing

Three types of panels were manufactured: (i) a quasi-isotropic panel with constant-stiffness, which served as the baseline, (ii) a variable-stiffness panel with complete overlaps (i.e., with 100% coverage) and (iii) a variable-stiffness panel with complete gaps (i.e., with 0% coverage). The stacking sequences for these tested panels are listed in Table 1. The fiber orientation notation used in Table 1 is that proposed by Gürdal and Olmedo [3]. One should note here that the studied variable-stiffness panels were optimized using the methodology and flow chart described in Ref. [5] to achieve a maximum buckling load compared to the baseline panel.

The fiber-steered panels were manufactured using a VIPER ® 4000 fiber placement machine. This AFP machine has the capability to lay-up any even number of 3.175 mm wide slit tape, up to 32 tows, and allows for individual tow cut/restart control. To manufacture the variable-stiffness composite laminates, each fiber-tow in the AFP process was laid up by following a predefined curvilinear-fiber path. To simulate the fiber paths, the ACE programming/simulation software was used. This software can also simulate the distribution of the AFP process-induced defects (see Fig. 1) and foresee the potential areas that might exhibit quality-related problems, resulted when the constraint of the minimum fiber radius of curvatures is violated. For a 3.175 mm wide prepreg tow, the minimum required radius of curvature, as recommended in the literature [32], is 635 mm for laying prepreg tows onto a surface free of wrinkles and micro-buckling.

All the tested panels were manufactured using G40-800/5276-1 carbon/epoxy slit tape from Cytec Engineered Materials. The panels were then cured at 177 °C in an autoclave for 2 h under a pressure of 0.58 MPa. The nominal material properties are listed in Table 2.

After being cured in the autoclave, the panels were cut into specimens with dimensions of 254 mm × 406 mm using a diamond saw under running water. Subsequently, the shorter edges of the trimmed specimens were machined flat and parallel to

Table 1
Stacking sequences of the tested panels.

Panel design	Stacking sequence
Quasi-isotropic design	$[+45/0/-45/90]_{2s}$
Overlaps design	$[\pm\langle 49\|41\rangle/\pm\langle 48\|61\rangle/\pm\langle 57\|73\rangle/\pm\langle 72\|77\rangle/]_s$
Gaps design	$[\pm\langle 49\|41\rangle/\pm\langle 48\|61\rangle/\pm\langle 57\|73\rangle/\pm\langle 72\|77\rangle/]_s$

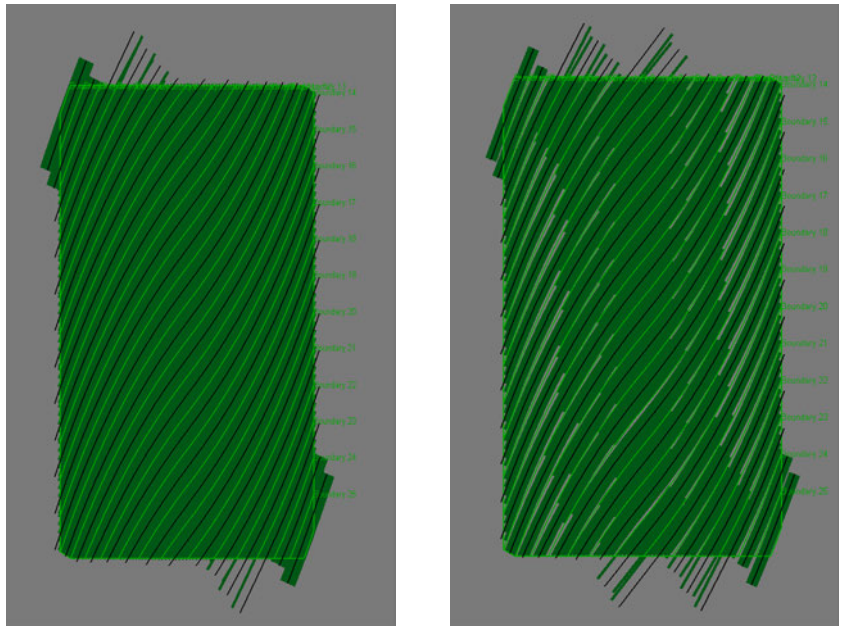

(a) (b)

Fig. 1. ACE simulation results: (a) complete overlaps and (b) complete gaps.

Table 2
Mechanical properties of G40-800/5276-1 unidirectional carbon/epoxy prepreg.

Moduli parameters		Strength parameters	
Longitudinal modulus, (E_1, GPa)	142.7	Longitudinal tension, (X^T, MPa)	3013
Transverse modulus, (E_2, GPa)	9.1	Longitudinal compression, (X^C, MPa)	1744
In-plane shear modulus, (G_{12}, GPa)	4.82	Transverse tension, (Y^T, MPa)	90
Major Poisson's ratio, (ν_{12})	0.3	Transverse compression, (Y^C, MPa)	200
		In-plane shear, (S^L, MPa)	170

ensure uniform end loading during the experiments. The configuration of a typical test specimen is shown in Fig. 2.

After the cutting of the panels, particular attention was devoted to measure the specimen-surface flatness. In fact, the out-of-flatness imperfections of rectangular thinwalled plates can be expected, even in isotropic materials, and are exacerbated by anisotropy and a distribution of random defects. Since the present investigation addresses the buckling phenomenon, which is related to out-of-plane deformations, it was crucial to measure the initial imperfections before testing the panels. For this purpose, the initial geometric imperfections of all the tested panels were measured with a CNC coordinated measuring machine (CNC Mitutoyo Mach 806)

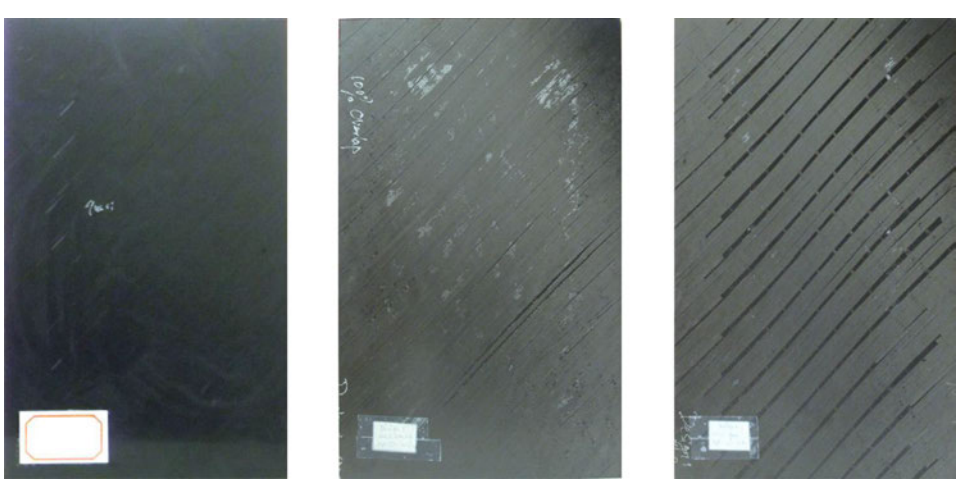

(a) (b) (c)

Fig. 2. Example of fiber steered composite panels: (a) quasi-isotropic panel, (b) panel with complete overlaps and (c) panel with complete gaps.

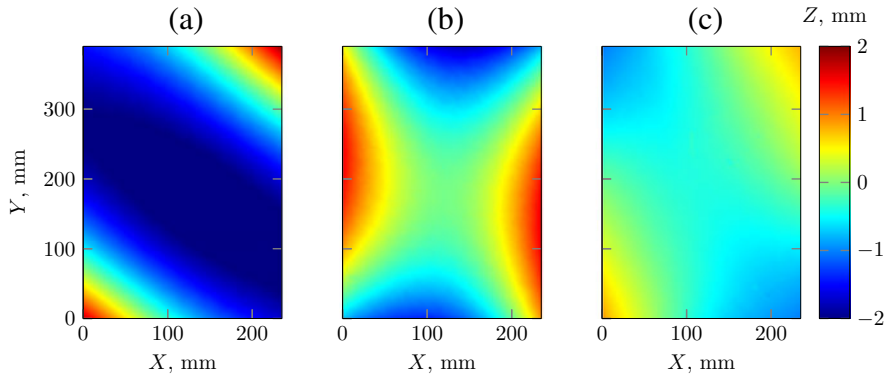

Fig. 3. Initial geometric imperfections measured in tested panels: (a) quasi-isotropic panel [R_{min} = −1.93, R_{max} = 1.78], (b) panel with complete overlaps [R_{min} = −1.62, R_{max} = 1.61] and (c) panel with complete gaps [R_{min} = −1.02, R_{max} = 0.94].

over a uniform grid with a spacing of 6.35 mm; the measurements were made in both in-plane directions. The data were then mapped using MATLAB® code based on the surf function. The results are shown in Fig. 3, here, R_{min} and R_{max} denote the lowest and the highest out-of-flatness imperfections, respectively, along the Z-axis (i.e., along the thickness direction).

Moreover, the weight, w_t, and the nominal thickness, h, of all of the tested panels were measured. The average measured values are summarized in Table 3, here, w^*, denotes the «weight index», which is defined as the ratio of the weight of a tested panel to the weight of the quasi-isotropic panel.

2.2. Experimental compression-buckling test set-up

A special mounting fixture was designed and manufactured to perform the compression-buckling tests. This fixture was designed with the aim to obtain the simply-supported edge-boundary conditions along all the four edges of the panels. These desired boundary conditions, which, in practice, are represented by a restrained out-of-plane displacement, free tangential edge rotations, and in-plane translational movements, are very difficult to replicate in laboratory. To overcome this issue, the edges of the panels were mounted between two knife-edge supports. A typical test specimen mounted in the support fixture is shown in Fig. 4. Furthermore, it is worth noting that a gap between the knife edges at both unloaded lateral sides of the panels was set to approximately 2-mm to allow free expansion.

Each tested panel was subjected to uniaxial compression by applying a uniform displacement along its horizontal top edge. The crosshead speed was fixed at 1 mm/min, and the loading was continued until the final failure of panel occurred. All the tests were performed at room temperature using an AMSLER machine provided with a 100-kN load cell.

2.3. Instrumentation and data acquisition

For data acquisition, sixteen axial strain gauges were installed to measure the axial strains as a function of the compressive load.

Table 3
Steered panels geometric characteristics.

Panel configuration	Weight, w_t[a] (kg)	w^* (−)	Thickness, h (mm)
Quasi-isotropic panel	0.386	1.00	2.51
Panel with complete overlaps	0.439	1.14	2.84
Panel with complete gaps	0.336	0.84	2.09

[a] Weight index.

Fig. 4. Test specimen mounted in the support fixture.

The typical locations of the back-to-back strain gauge pairs are shown in Fig. 5. For all gauges, which were 6-mm long, the electrical resistance was 350 Ω and the gauge factor was 2.1. In addition, four non-contact laser displacement sensors with a high spatial resolution (8 μm) and a large working distance (30–80 mm) were used to record the out-of-plane panel deflection during the experiments. These sensors were focused on the vertical mid-spans of the panels, as shown in Fig. 6. During the experiment, data from the strain gauges, the laser sensors out-of-plane displacement, the compressive load, and the in-plane applied displacement were recorded at regular intervals using custom-written LabVIEW ® software. Note that the strain gauges and the non-contact laser sensors were set to zero, before applying any displacement to the panel.

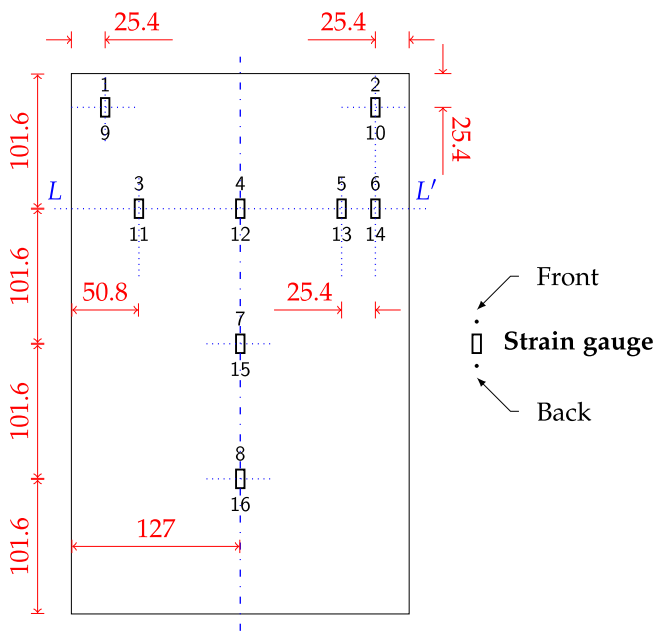

Fig. 5. Locations of strain gauges (all dimensions in millimeters).

3. Experimental results and discussions

3.1. Load vs. displacement response

Fig. 7 shows the load vs. displacement responses of the tested panels. The panel configurations under investigation exhibited the same general pattern behavior. For ease of discussion, the overall load vs. displacement responses of the panels are divided into four zones, as identified in Fig. 7, which are as follows:

- Zone-I: Initial non-linear zone
- Zone-II: Pre-buckling zone
- Zone-III: Transition zone
- Zone-IV: Post-buckling zone

Zone-I, the initial non-linear zone, is typically observed during uniaxial tensile and/or compression tests and does not reflect the real material behavior. For instance, the ASTM-D695 compressive test describes zone-I as "*an artifact caused by a take-up of slack and alignment or seating of the specimen*". Further, the same standard advises that "*to obtain correct values of such parameters as modulus, strain, and offset yield point, this artifact must be compensated for to give the corrected zero point on the strain or extension axis*". In the present investigation, the load–displacement curves were not corrected as advised in some ASTM standards, including the ASTM-D695. This choice was dictated by the fact that this investigation is dealing with non-standard and large specimens and imperfect flat panels, and as such, it was difficult to ascertain whether all initial non-linear behavior was an artifact. Indeed, zone-I extended to approximately 2 kN for the quasi-isotropic panel and the variable-stiffness panel with complete gaps (see Fig. 7a and c). Nonetheless, for the panel with overlaps, this initial non-linearity extended to approximately 3 kN (see Fig. 7b). In the authors' opinion, the extent of this initial zone does not depend on the nature of the material (i.e., constant- or variable-stiffness) but rather on the initial geometrical imperfections of the loading-surface.

Zone-II, the pre-buckling zone, was characterized by a linear elastic response, which reflects the real material behavior. This part of the curve was used to extract the compressive pre-buckling stiffness value, K_0, for the three investigated panel configurations. Hence, the experimental pre-buckling stiffnesses were calculated from the best-fit slope of the linear zone-II of the load–displacement curve, and the results are presented in Table 4. To highlight the effects of the curvilinear-fiber concept, the results were normalized with respect to the properties of the quasi-isotropic panel, and are presented in parentheses in Table 4. It can be seen from the normalized data that the pre-buckling stiffness of the panel with overlaps increased by approximately 64% while that for the panel with gaps decreased slightly (by approximately 7%). However, with respect to the baseline panel (i.e., the quasi-isotropic panel), the thickness of the panel with gaps decreased, while that for the panel with overlaps increased, as shown previously in Table 3. Consequently, the experimental

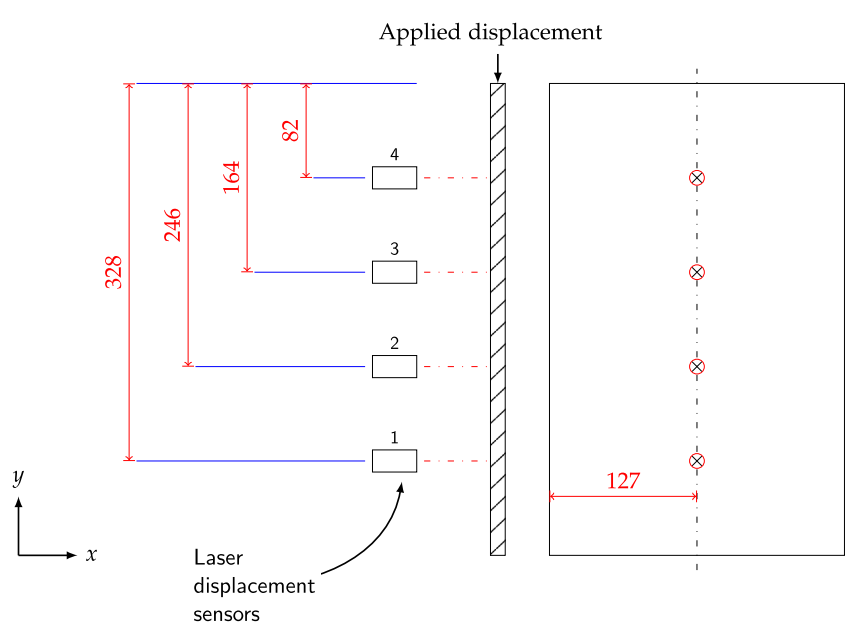

Fig. 6. Laser displacement sensors locations (all dimensions in millimeters).

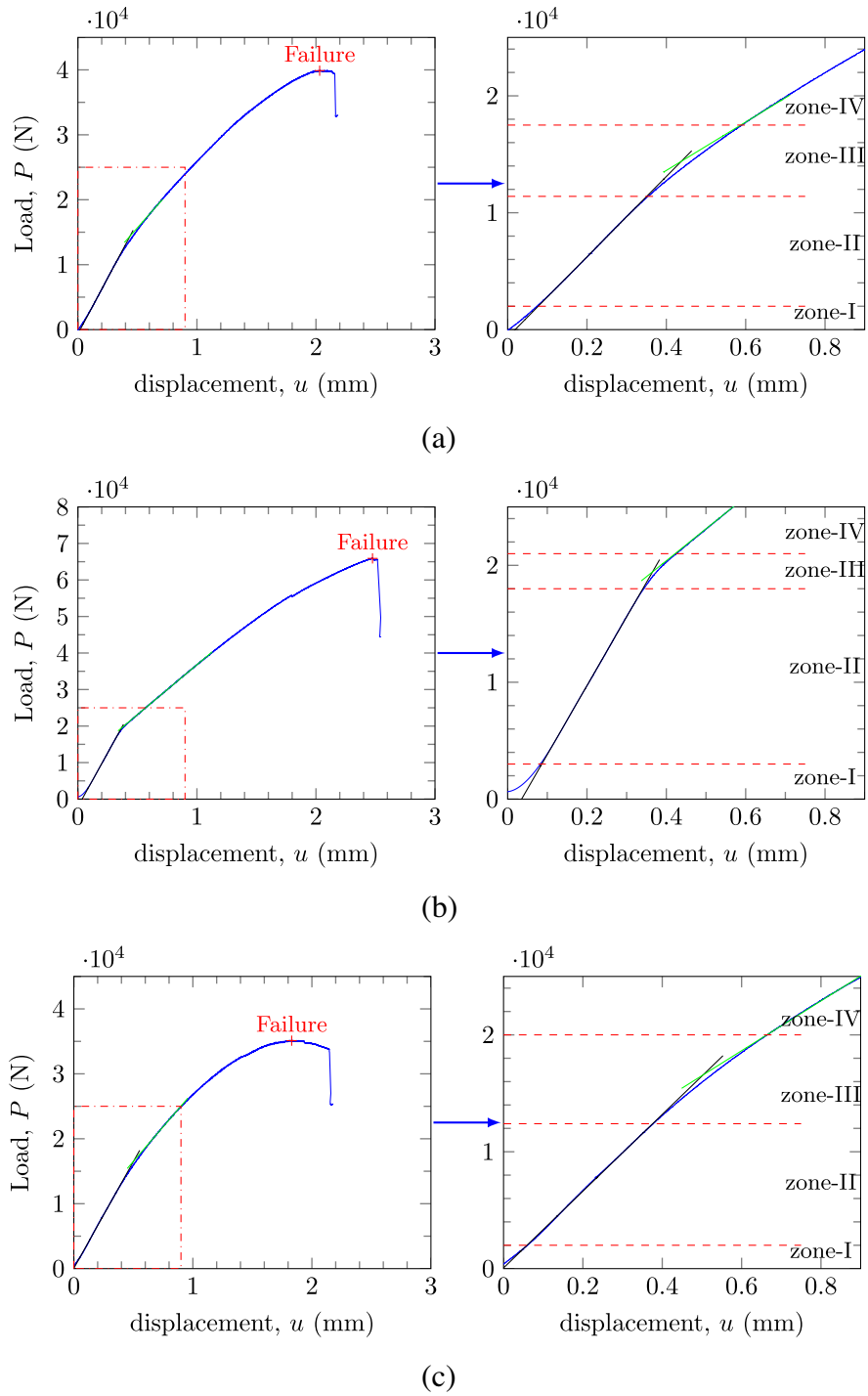

Fig. 7. Load versus in-plane displacement curves for the tested panels: (a) quasi-isotropic panel, (b) panel with complete overlaps and (c) panel with complete gaps.

Table 4
Buckling characteristics of the steered panels.

Panel configuration	K_0 [kN/mm]	P_{cr} [kN]	P_u [kN]	R_u [N/mm^2]
Quasi-isotropic panel	34.59 (**1.00**)[a]	11.52 (**1.00**)	39.87 (**1.00**)	62.64 (**1.00**)
Panel with complete overlaps	56.61 (**1.64**)	18.97 (**1.65**)	65.91 (**1.65**)	91.13 (**1.45**)
Panel with complete gaps	32.21 (**0.93**)	12.19 (**1.06**)	35.11 (**0.88**)	65.75 (**1.05**)

[a] Values in parentheses are the normalized values.

results should be corrected using the panel thickness to provide a true indication of the effect of the curvilinear-fiber concept.

Unfortunately, the thicknesses of manufactured fiber-steered panels are inherently not uniform. This non-uniformity is attributed in part to the local defects associated with the manufacturing process. Therefore, as an alternative, the results were corrected using the «weight index», w^*, values of the panels by taking onto account the fact that their lengths and widths are nearly the same. In fact, as shown in Table 3, the panel with gaps is lighter than the quasi-isotropic panel and the panel with overlaps by 13% and 33%, respectively. These differences in the weights will obviously affect

the buckling characteristics of the steered panels, as shown in Table 5; here, *EA*, denotes the pre-buckling extensional stiffness values obtained by multiplying the pre-buckling stiffness by the nominal panel length. The results presented in Table 5 indicate that the weight-normalized pre-buckling extensional stiffness was 1.45 times greater for the panel with overlaps and 1.08 times greater for the panel with gaps.

Zone-III, the critical transition zone, is where buckling occurs and where the critical buckling load, P_{cr}, should be identified and recorded. For a perfect panel (i.e., ideal panel), the critical buckling load can be distinctly identified from the load–displacement curve as a bifurcation point. However, as is well recognized, the exact start of the buckling process on the load–displacement curve for an imperfect panel (i.e., real panel) is difficult to as-certain. Indeed, a number of factors have a considerably effect on the buckling test in experiments. These include the geometric and/or material non-linearities in the tested panel, the accuracy of the testing machine, and whether the correct mounting fixture has been used or not (using an improper fixture can cause a misalignment between the load direction and the tested panel). Thus, a transition zone instead of a distinct bifurcation point is seen in a real test. In the present study, the transition zone was defined as the portion of the load–displacement curve between the two tangent lines to the curve in zone-II and zone-IV (see Fig. 7). Unfortunately, there is a lack of agreement regarding how best to determine the buckling load from the experimental data curves. For example, one possible approach is to define the critical buckling load point as the vertical projection of the intersection point of the tangent lines mentioned previously onto the experimental data curve. However, the manner in which the tangent to the post-buckling curve is identified, is generally more dependent an individual judgment. To overcome this issue, a conservative approach has been used herein to extract the experimental buckling load value from the load–displacement curve; the buckling load was defined as corresponding to the point where the load–displacement curve first deviated from the linear zone-II and moved into zone-III. To ensure that the experimental buckling loads for all the tested panels could be determined with ease, the buckling load was defined to be that where the best-fit slope corresponding to the linear pre-buckling zone of the load–displacement curve was approximately 0.998. According to this criterion, all the experimental buckling loads were extracted and the obtained data are summarized in Table 4. As can be seen from the table, the panel with overlaps exhibited the highest critical buckling load (18.97 kN), which is approximately 65% higher than that of the baseline panel (11.52 kN). For the panel with gaps, a modest increase (6%) in the critical buckling load was observed. The experimental buckling load values were afterward corrected with the «weight index», and the results are shown in Table 5. It can be seen from these results that the weight-normalized buckling loads of the panels with overlaps and gaps were higher by 45% and 22%, respectively, than that of quasi-isotropic panel. These results are consistent with previous research results [26–29], which demonstrate the possibility to enhance the buckling characteristics of the composites structures, with respect to the baseline panel, using an optimum curvilinear-fiber design.

Table 5
Weight-normalized buckling characteristics of the steered panels.

Panel configuration	*EA* [10^6 N]	EA/w^* [10^6 N]	P_{cr}/w^* [kN]	P_u/w^* [kN]	R_u/w^* [N/mm^2]
Quasi-isotropic panel	13.95 (**1.00**)[a]	13.95 (**1.00**)	11.52 (**1.00**)	39.87 (**1.00**)	62.64 (**1.00**)
Panel with complete overlaps	23.12 (**1.66**)	20.33 (**1.46**)	16.68 (**1.45**)	57.95 (**1.45**)	80.13 (**1.28**)
Panel with complete gaps	13.11 (**0.94**)	15.06 (**1.08**)	14.01 (**1.22**)	40.33 (**1.01**)	75.53 (**1.21**)

[a] Values in parentheses are the weight-normalized values.

Zone IV, the post-buckling zone, is where material loses its initial stiffness but continues to handle the load to higher values. The ultimate loads of the panels are indicated by the "+" symbol in the load–displacement curves shown in Fig. 7, and the exact values are listed in Table 4. It can be seen from the data that the panel with overlaps exhibited the most significant improvement in load-carrying capacity (i.e., an improvement of 65% over that of a quasi-isotropic panel). In contrast, the panel with gaps failed at a load 12% lower than that at which the quasi-isotropic panel did. However, on the basis of the «weight index» values, the weight-normalized failure load for panel with gaps was found to be the same as that of the baseline panel (see Table 5). In contrast, the weight-normalized failure load for the panel with overlaps was 45% higher than that of the quasi-isotropic panel as well as that of the panel with gaps.

The values in the last column in Table 4 represent the ultimate buckling strength, R_u, values of the tested panels. As shown, the panel with overlaps exhibited the highest ultimate strength (91 N/mm^2), which was approximately 45% higher than the values of the other two equally strong panels (i.e., the quasi-isotropic panel and the panel with gaps). However, when compared to the baseline panel, the variable-stiffness panels with overlaps and gaps exhibited weight-normalized ultimate strengths that were higher by 28% and 21%, respectively (see Table 5).

It is also interesting to note that the post-buckling behavior of the two variable-stiffness panels was characterized by a small local-failure, which was indicated by the first slight drop in load, as can be seen from the load–displacement curves in Fig. 7b and c. This drop was accompanied by an audible noise. However, no visible damage was observed during the buckling test. This drop occurred at approximately 56 kN (approximately 294% of the buckling load) for the panel with overlaps and at 33 kN (approximately 268% of the buckling load) for the panel with gaps. Note that the drop in load was more pronounced in the variable-stiffness panel with overlaps (approximately 13%). The displacement corresponding to this local-failure load is equal to 1.817 mm (corresponding to approximately 0.44% axial strain) and 1.419 mm (corresponding to approximately 0.35% axial strain) for the panel with overlaps and the panel with gaps, respectively. However, for the quasi-isotropic panel, no indication of local-failure was observed until the overall failure.

From the weight-normalized results shown in Table 5, it is clear that the variable-stiffness panel with overlaps exhibited significantly higher improvements in performance than did the panel with gaps. In particular, the weight-normalized pre-buckling extensional stiffness, the weight-normalized buckling load, and the weight-normalized failure load of the panel with overlaps were 35%, 19%, and 44% higher, respectively. From these results, it has been demonstrated that by using the coverage method, it is possible to eliminate the formation of gaps between adjacent tow-courses without generating successive overlaps (which results in a significant thickness build-up in the finished panel) as is the case for Ref. [26]. In contrast to the overlaps design tested in Ref. [26] (which is discussed in Section 1), it was found that the overlap design strategy adopted in the current study resulted in the minimum possible amount of overlaps while leading to a better performance than those of the quasi-isotropic panel and the panel with complete gaps (0% coverage).

3.2. Out-of-plane deflection

As mentioned earlier, four non-contact laser displacement sensors were used to monitor the deformed shape progression of the

tested panels. The locations of these lasers sensors can be seen in Fig. 6. As per the sensor arrangement, negative recorded values indicated that the panel was approaching the sensor, while positive values indicated that the panel was moving away from the sensor.

Fig. 8 shows the out-of-plane deflection, w, as measured at the longitudinal centerline of the panels using the non-contact laser sensors placed as per the schematic shown in Fig. 6. In Fig. 8, the out-of-plane deflection, w, was normalized using the nominal panel thickness, h. The dots refer to the exact actual four measurements, while the solid lines represent the best-fit to describe the entire panel behavior. To be able to observe how the out-of-plane deflections evolved during the compression-buckling test, three load (P) levels were chosen relative to the critical buckling load (P_{cr}), such that the ratio r_p (=P/P_{cr}) was 0.5, 1.0 and 2.0. These load ratios covered the entire region of the panel behavior from the linear pre-buckling zone up to the post-buckling zone.

The obtained results indicated that, at a low load ratio (i.e., for $r_p = 0.5$), a small deflection was detected in all the AFP tested panels. This was certainly owing to the initial geometric imperfections in the panels, as shown previously in Fig. 3. In addition, it can be noticed from Fig. 8b that the out-of-plane deflections were less pronounced for the panel with overlaps, which was relatively thicker than the other two panels. In fact, the maximum out-of-plane deflection, which occurred at the buckling load (i.e., at $r_p = 1$), was observed in the case of the panel with gaps and was approximately twice the nominal thickness of the panel. One possible explanation for this result is the difference in the flexural stiffnesses of the panels. Both the quasi-isotropic panel and the panel with gaps buckled globally in the form of a half sine wave at their longitudinal centerline. In contrast, the panel with overlaps buckled globally into two half sine waves at the longitudinal centerline (i.e., into two regions moving in opposite directions, with there being no displacement along the horizontal centerline of the panel). It should also be noted that the global buckling modes did not change as the load was increased. A proportional increase in the amplitude of the out-of-plane deflection was observed as the compressive load was increased.

3.3. Strain gauges

Sixteen strain gauges were installed back-to-back on the surfaces of the tested panels, in order to measure the axial strains as function of the compressive load (see Fig. 5). A typical example of the entire set of responses of these strain gauges during the compression-buckling tests is presented in Fig. 9 at the strain gauge locations (G4-12) for the panel with overlaps.

In the following subsections, selected strains results (G3-11, G4-12, G5-13 and G6-14) are discussed in terms of the membrane strain, defined as the average strain from a back-to-back pair of strain gauges, and the bending strain, defined as the difference in the values measured by the back-to-back strain gauges.

3.3.1. Membrane strains

Fig. 10a and b depict the distribution of the axial membrane strains along the horizontal line, LL', (see Fig. 4) for the panels with overlaps and gaps, respectively. An increasing load levels have been selected to provide a comprehensive view about the entire panels' behavior throughout the different aforementioned load–displacement zones.

For the panel with overlaps (see Fig. 10a), the axial membrane strain distribution was almost uniform along the panel's width throughout the entire pre-buckling zone and until the critical buckling load. Further, it can be seen that the strain was re-distributed

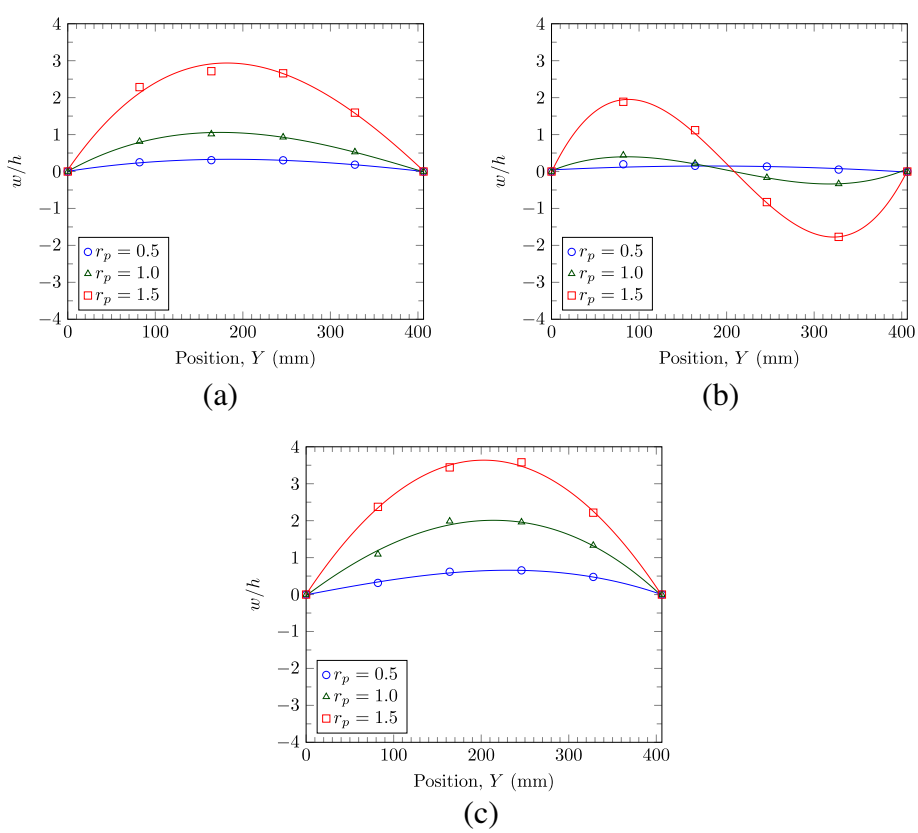

Fig. 8. Normalized out-of-plane deflection (w/h) vs. laser locations for different loadratios (r_p): (a) quasi-isotropic panel, (b) panel with complete overlaps and (c) panel with complete gaps.

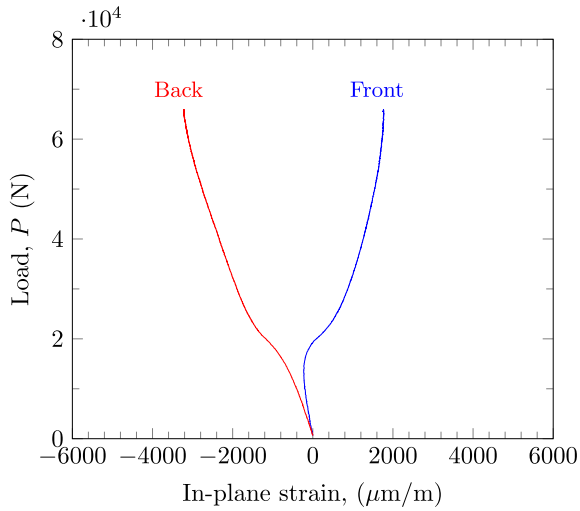

Fig. 9. Load versus in-plane strain at panel with complete overlaps at gauge locations 4 and 12.

towards the panel edges after buckling. This observation is in agreement with the results reported by Starnes and Rouse [33] regarding the buckling behavior of a rectangular carbon/epoxy plate. They found that the membrane strains typically shift from the panel's axial centerline towards its unloaded edges at or near the buckling load. However, Wu et al. [26] in their experimental work on variable-stiffness panels, observed that the strain redistribution load can occur at loads higher than the critical buckling load. They suggested that this behavior is prompted by the additional axial stiffening provided by the tow-overlaps along the panel's unloaded edges. This variance in the axial membrane strains was attributed to the differences in the manufacturing strategies used. Indeed, it should be remembered that the AFP panels tested in the present investigation are manufactured in such a way that excessive overlap accumulation did not occur.

Fig. 10a also reveals that, after the buckling event, the axial membrane strain at the panel's vertical centerline (i.e., at gauge location 4) remained nearly constant over the entire post-buckling zone, while it amplifies at the remaining gauge locations (i.e., at gauge locations 3, 5, and 6). The largest variation in membrane strain was recorded for the strain gauges at location 6 (25.4-mm to the left

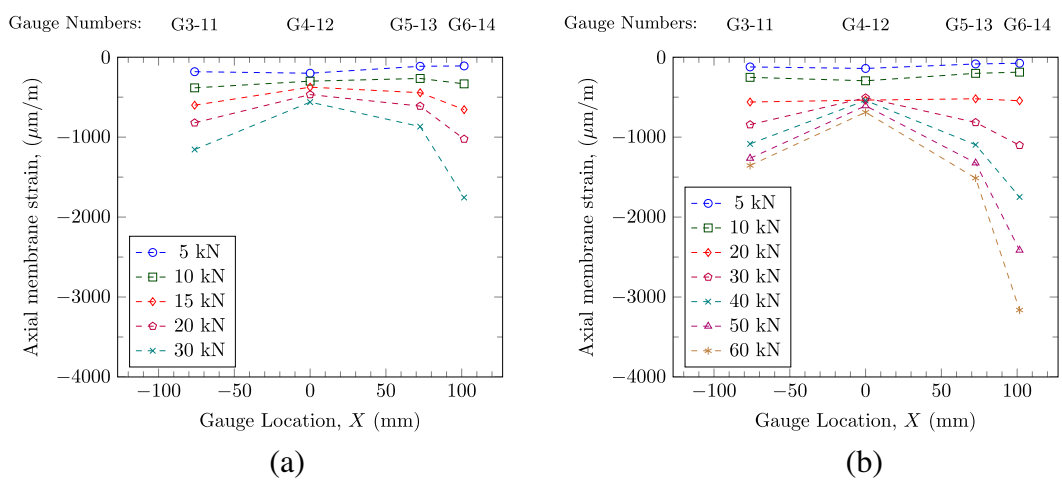

Fig. 10. Axial membrane strains for variable-stiffness panels: (a) panel with complete overlaps, and (b) panel with complete gaps.

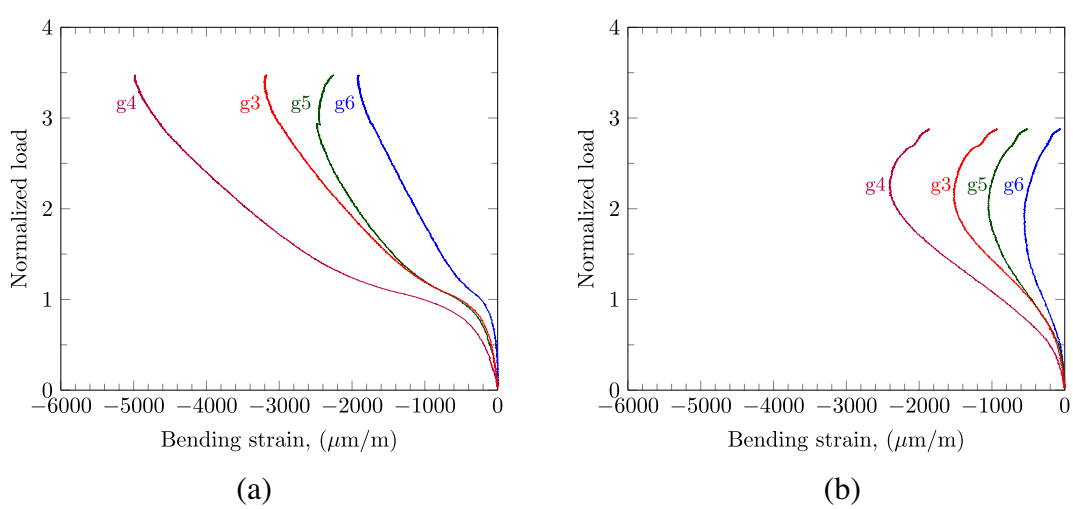

Fig. 11. Bending strains for variable-stiffness panels: (a) panel with complete overlaps, and (b) panel with complete gaps.

unloaded simply-supported edge). At this location, the recorded membrane strain at a load of 60 kN was 6 times greater than the one recorded at a load of 20 kN.

A comparison between the variable-stiffness panels' behavior at low-load levels from Fig. 10a and b, revealed that the distribution of the pre-buckling membrane strains in the panel with gaps was not as uniform as than in the panel with overlaps. Furthermore, a small asymmetry in the membrane strain readings was observed for the panel with gaps. This asymmetry is characterized by the strain gauges readings at location 3 being higher than those at location 5. This may be caused by the residual stresses induced by mounting of the panels in the test fixture. However, in spite of this initial asymmetrical distribution, it was clear that the membrane strains shift from the panel's axial centerline towards the lateral edges at load levels close to the buckling load. For a load of 30 kN, the strain gauge pairs at location 6 showed an average value 5.25 times greater than the value recorded for a load of 20 kN.

3.3.2. Bending strains

Fig. 11a and b show the bending strain readings at different gauges locations for the panels with overlaps and gaps, respectively. The compressive load was normalized with respect to the buckling load for each panel. As shown, for both variable-stiffness panels, the bending strain was very low at the unloaded simply-supported edge (i.e., at location 6) and increased to its maximum value at the panel center near the point of maximum out-of-plane deflection (i.e., at location 4). This behavior suggests that there was no edge effect during the buckling experiment. On the other hand, the bending strain graphs for the gauges at locations 3 and 5 were similar until buckling occurred.

For the panel with gaps (see Fig. 11b), there was a slight reversal in the sign of the tangents to the bending strain curves at a load approximately 2 times the buckling load. The same phenomenon also observed for the panel with overlaps in the gauges at location 5, this happened at a load approximately 3 times the buckling load. When viewed along with the load–displacement data, it can be concluded that this phenomenon is probably owing to the occurrence of local internal damage.

4. Conclusions

In this work, a detailed experimental investigation was conducted to characterize the buckling behavior of simply-supported rectangular variable-stiffness panels subjected to a uniform end-shortening. Two optimum variable-stiffness designs with a minimum possible amount of AFP defects were manufactured using the tow-drop method: one with 0% coverage (i.e., complete gaps) and the other with 100% coverage (i.e., complete overlaps). A quasi-isotropic laminate with constant-stiffness was also manufactured to serve as the baseline panel. Prior to testing, the weights, nominal thicknesses, and initial geometric imperfections of the cured panels were measured. A special mounting fixture enabling the simply-supported boundary conditions on all panel edges was manufactured and used for the compression-buckling tests, which were performed in the displacement control mode. Sixteen unidirectional strain gauges were installed to measure the axial strains at different locations on the steered panels. In addition, four non-contact laser displacement sensors were used to observe the axial centerlines of the panels and monitor the evolution of their buckling shapes.

The experimental results indicated clearly that the variable-stiffness panels with overlaps or gaps exhibit better structural performance compared to the quasi-isotropic baseline panel. When weight-normalized, the pre-buckling stiffness, buckling load, and failure load of the panel with overlaps were higher by 35%, 19% and 44%, respectively, than those of the panel with gaps. Further, a small local failure was observed in the case of the variable-stiffness panels in the post-buckling zone. The strain gauges data indicated that the unloading simply supported edges did not affect the buckling behavior. The initial geometric imperfections of the panels had a significant effect on their buckling shapes. Indeed, the data from the non-contacting displacement laser sensors indicated that both the baseline panel and the panel with gaps buckled globally into a half sine wave at the longitudinal centerline, while the panel with overlaps buckled globally into two half sine waves. Further, it was also found that the buckling shapes did not change with an increase in the applied load.

Acknowledgments

The authors acknowledge the financial support provided by the Natural Sciences and Engineering Research Council of Canada (NSERC) and the Consortium for Research and Innovation in Aerospace in Québec (CRIAQ). We are very thankful to Prof. Pasini, Dr. M.A. Nik, and Dr. K. Fayazbakhsh for computing the optimal variable-stiffness laminate layups. We are also very grateful for Bombardier Aerospace and Composites Atlantic Limited for their support.

References

[1] Dirk H-JL, Ward C, Potter KD. The engineering aspects of automated prepreg layup: history, present and future. Compos Part B Eng 2012;43:997–1009.
[2] Gürdal Z, Olmedo R. Composite laminates with spatially varying fiber orientations: variable stiffness panel concept. In: Proceedings of the AIAA/ASME/ASCE/AHS/ASC 33rd structures, structural dynamics and materials conference. Dallas, TX; 1992. p. 798–808.
[3] Gurdal Z, Olmedo R. In-plane response of laminates with spatially varying fiber orientations-variable stiffness concept. AIAA J 1993;31:751–8.
[4] Gürdal Z, Tatting BF, Wu C. Variable stiffness composite panels: effects of stiffness variation on the in-plane and buckling response. Compos Part A: Appl Sci Manuf 2008;39:911–22.
[5] Nik MA, Fayazbakhsh K, Pasini D, Lessard L. Surrogate-based multi-objective optimization of a composite laminate with curvilinear fibers. Compos Struct 2012;94:2306–13.
[6] Hyer M, Lee H. The use of curvilinear fiber format to improve buckling resistance of composite plates with central circular holes. Compos Struct 1991;18:239–61.
[7] Setoodeh S, Abdalla MM, IJsselmuiden ST, Gürdal Z. Design of variable-stiffness composite panels for maximum buckling load. Compos Struct 2009;87:109–17.
[8] Wu Z, Weaver PM, Raju G. Postbuckling optimisation of variable angle tow composite plates. Compos Struct 2013;103:34–42.
[9] Lopes C, Gürdal Z, Camanho P. Variable-stiffness composite panels: buckling and first-ply failure improvements over straight-fibre laminates. Comput Struct 2008;86:897–907.
[10] Lopes C, Gürdal Z, Camanho P. Tailoring for strength of composite steered-fibre panels with cutouts. Compos Part A: Appl Sci Manuf 2010;41:1760–7.
[11] Khani A, IJsselmuiden S, Abdalla M, Gürdal Z. Design of variable stiffness panels for maximum strength using lamination parameters. Compos Part B: Eng 2011;42:546–52.
[12] Abdalla MM, Setoodeh S, Gürdal Z. Design of variable stiffness composite panels for maximum fundamental frequency using lamination parameters. Compos Struct 2007;81:283–91.
[13] Akhavan H, Ribeiro P. Natural modes of vibration of variable stiffness composite laminates with curvilinear fibers. Compos Struct 2011;93:3040–7.
[14] Ribeiro P, Akhavan H. Non-linear vibrations of variable stiffness composite laminated plates. Compos Struct 2012;94:2424–32.
[15] Blom AW, Stickler PB, Gürdal Z. Optimization of a composite cylinder under bending by tailoring stiffness properties in circumferential direction. Compos Part B: Eng 2010;41:157–65.
[16] Khani A, Abdalla M, Gürdal Z. Optimum tailoring of fibre-steered longitudinally stiffened cylinders. Compos Struct 2015;122:343–51.
[17] Rouhi M, Ghayoor H, Hoa SV, Hojjati M. Multi-objective design optimization of variable stiffness composite cylinders. Compos Part B: Eng 2015;69:249–55.
[18] Sawicki A, Minguet P. The effect of intraply overlaps and gaps upon the compression strength of composite laminates. In: The 39th AIAA structural, dynamics, & materials conference. Long Beach, CA; 1998. p. 744–54.
[19] Turoski LE. Effects of manufacturing defects on the strength of toughened carbon/epoxy prepreg composites [Master of Science]. Bozeman: Montana State University, Mechanical Engineering; 2000.
[20] Croft K, Lessard L, Pasini D, Hojjati M, Chen J, Yousefpour A. Experimental study of the effect of automated fiber placement induced defects on

performance of composite laminates. Compos Part A: Appl Sci Manuf 2011;42:484–91.
[21] Legay P, Boukhili R, Hojjati M, Chen J. Impact and compression behaviour of AFP manufactured carbon/epoxy composites containing gaps and overlaps. In: 26th annual technical conference of the American society for composites and the 2nd joint US-Canada conference on composites. Montreal, Quebec, Canada; 2011. p. 1163–79.
[22] Fayazbakhsh K, Prabhakar S, Pasini D, Lessard L. A study of the influence of gaps and overlaps on the strength of composite panels made by Automated Fiber Placement. In: 26th annual technical conference of the american society for composites and the 2nd joint US-Canada conference on composites. Montreal, Quebec, Canada; 2011.
[23] Fayazbakhsh K, Nik MA, Pasini D, Lessard L. Defect layer method to capture effect of gaps and overlaps in variable stiffness laminates made by automated fiber placement. Compos Struct 2013;97:245–51.
[24] Nik MA, Fayazbakhsh K, Pasini D, Lessard L. Optimization of variable stiffness composites with embedded defects induced by automated fiber placement. Compos Struct 2014;107:160–6.
[25] Ribeiro P, Akhavan H, Teter A, Warmiński J. A review on the mechanical behaviour of curvilinear fibre composite laminated panels. J Compos Mater 2013;48:2761–77.
[26] Wu KC, Gürdal Z, Starnes JH. Structural response of compression-loaded, tow-placed, variable stiffness panels. In: Proceedings of the AIAA/ASME/ASCE/AHS/ASC 43rd structures, structural dynamics and materials conference. Denver, CO, USA; 2002. p. 2002-1512.
[27] Wu KC, Gürdal Z. Variable stiffness panel structural analyses with material nonlinearity and correlation with tests. In: Proceedings of the 47th AIAA/ASME/ASCE/AHS/ASC structures, structural dynamics and materials conference. Newport, RI; 2006.
[28] Jegley DC, Tatting BF, Gürdal Z. Optimization of elastically tailored tow-placed plates with holes. In: Proceedings of the AIAA/ASME/ASCE/AHS/ASC 44th structures, structural dynamics and materials conference. Norfolk, Virginia; 2003. p. 2003-1420.
[29] Jegley DC, Tatting BF, Gürdal Z. Tow-steered panels with holes subjected to compression or shear loading. In: Proceedings of the AIAA/ASME/ASCE/AHS/ASC 46th structures, structural dynamics and materials (SDM) conference. Austin, Texas; 2005. p. 2005–17.
[30] Tatting BF, Gürdal Z. Design and manufacture of elastically tailored tow placed plates. Tech. Rep., NASA, Langley Research Center, Hampton, VA, NASA/CR-2002-211919; 2002.
[31] Tatting BF, Gürdal Z. Automated finite element analysis of elastically-tailored plates. Tech. Rep., NASA, Langley Research Center, Hampton, VA, NASA/CR-2003-212679; 2003.
[32] Nagendra S, Kodiyalam S, Davis JE, Parthasarathy V. Optimization of tow fiber paths for composite design. In: Proceedings of the AIAA/ASME/ASCE/AHS/ASC 36th structures, structural dynamics and materials conference. New Orleans, LA; 1995. p. 1031–41.
[33] Starnes Jr JH, Rouse M. Postbuckling and failure characteristics of selected flat rectangular graphite-epoxy plates loaded in compression. AIAA Paper 1981;81:423–34.